Contents lists available at ScienceDirect

Chemical Engineering Journal

journal homepage: www.elsevier.com/locate/cej

Self-assembling peptide hydrogels facilitate vascularization in two-component scaffolds

Zain Siddiqui [a,1], Biplab Sarkar [a,1], Ka Kyung Kim [a], Arjun Kumar [a], Reshma Paul [a], Aryan Mahajan [a], Jonathan M. Grasman [a], Jian Yang [b], Vivek A. Kumar [a,c,d,*]

[a] Department of Biomedical Engineering, New Jersey Institute of Technology, Newark, NJ, USA
[b] Department of Biomedical Engineering, Huck Institutes of The Life Sciences, Materials Research Institute, Pennsylvania State University, University Park, PA, USA
[c] Department of Chemical & Materials Engineering, New Jersey Institute of Technology, Newark, NJ, USA
[d] Department of Restorative Dentistry, Rutgers School of Dental Medicine, Newark, NJ, USA

ARTICLE INFO

ABSTRACT

One of the major constraints against using polymeric scaffolds as tissue-regenerative matrices is a lack of adequate implant vascularization. Self-assembling peptide hydrogels can sequester small molecules and biological macromolecules, and they can support infiltrating cells in vivo. Here we demonstrate the ability of self-assembling peptide hydrogels to facilitate angiogenic sprouting into polymeric scaffolds after subcutaneous implantation. We constructed two-component scaffolds that incorporated microporous polymeric scaffolds and viscoelastic nanoporous peptide hydrogels. Nanofibrous hydrogels modified the biocompatibility and vascular integration of polymeric scaffolds with microscopic pores (pore diameters: 100–250 μm). In spite of similar amphiphilic sequences, charges, secondary structures, and supramolecular nanostructures, two soft hydrogels studied herein had different abilities to aid implant vascularization, but had similar levels of cellular infiltration. The functional difference of the peptide hydrogels was predicted by the difference in the bioactive moieties inserted into the primary sequences of the peptide monomers. Our study highlights the utility of soft supramolecular hydrogels to facilitate host-implant integration and control implant vascularization in biodegradable polyester scaffolds in vivo. Our study provides useful tools in designing multi-component regenerative scaffolds that recapitulate vascularized architectures of native tissues.

1. Introduction:

Acellular biomaterials [1] have been demonstrated to heal some of the most challenging tissue injuries — central nervous system injury [2], critical-sized bone defect [3], ischemic tissue damage [4,5], and volumetric muscle loss [6,7]. Such implantable biomaterial scaffolds can facilitate tissue healing and regeneration after sterile injuries [2,8] or pathogenic infections [9,10]. One of the issues preventing large-scale adoption of such scaffolds is the lack of host-implant integration, deposition of native extracellular matrix (ECM) within scaffolds, and a lack of implant vascularization [11–14]. Here, we report a strategy to tackle these challenges in a polymeric scaffold, based on functionalized self-assembling peptide hydrogels.

After biomaterial scaffolds are implanted in vivo, they can either be walled off from the host by fibrous encapsulation [15–17], or integrate dynamically with the host tissue via tunable biodegradation, cellular infiltration, scaffold-based signaling, vascularization/innervation, and optionally, release of sequestered factors [5,18,19]. The integration of such implants with the surrounding host tissue can be hampered by low cellular infiltration and a lack of vascularization inside the implant.

Metabolic function of the cells inside the implant requires an adequate supply of oxygen and nutrients such as glucose and glutamine, which cannot be transported efficiently by diffusion in > 1 mm sized implants. There are a variety of strategies to encourage microvascular perfusion of implants, such as pro-angiogenic scaffolds [5,20], bioactive factors [21,22], transplanted cells [23], monocyte-recruiting thin films

[24], and T_H2 cell recruiting antigens [25]. A platform system that can tune biological response to scaffolds, resulting in angiogenesis, would increase the regenerative efficacy of acellular biomaterials.

2. Model System:

Here, we develop a two-component scaffold that combines poly (octamethylene citrate) (POC) scaffolds and nanofibrous self-assembling peptide hydrogels to achieve *tunable* implant vascularization *in vivo*. POC scaffolds [26] are solid microporous materials that have been used for repair and regeneration of cartilage [27,28] and urinary bladder smooth muscle [29]. The biodegradation of citrate-based scaffolds releases citric acid, which can enter nearby cells and act as a metabolic fuel [30]. In contrast, supramolecular peptide hydrogels are soft viscoelastic matrices self-assembled from short biofunctional peptides that mimic the ultrastructure of the extracellular matrix [2,4,5,10,19,31–35].

In this work, we aimed to improve the bio-integration of polymeric implants *without* built-in vasculature [36,37], by generating composite matrices that non-covalently functionalize POC scaffolds with supramolecular peptide hydrogels with differing angiogenic properties (Table 1, Fig. 1). We hypothesized that such hybridized matrices would lead to enhanced cellular infiltration after implantation *in vivo* in comparison to pristine POC scaffolds.

Both of the peptides selected (SLan and SLKr5, Table 1) possess identical amphipathic self-assembling domain [K(SL)$_6$K] attached via glycine linkers to angiogenic [4,5,35] or anti-angiogenic [33] domains (Fig. 1). The angiogenic peptide SLan has a terminal VEGF-mimic domain which stimulates angiogenesis of proliferating endothelial cells [35], while the Kringle-5 mimic within the SLKr5 peptide inhibits endothelial cell proliferation [33]. We show that both hydrogels facilitate cellular infiltration within the polymeric scaffold, whereas SLan was dramatically better at promoting angiogenic sprouting within the scaffold pores. Our results demonstrate the initial steps in developing vascularizing hydrogels [38] that may find utility in engineering vascularized tissues [11], and in improving clinical success rates for biomaterial implants and artificial organs [13,14,39].

3. Methods:

3.1. Preparation of microporous polymeric scaffolds

Poly(octamethylene citrate) (POC) pre-polymer was prepared by dissolving 1,8-octanediol and adding citric acid at 160 °C and maintained at 140 °C for 1 h of polymerization [40]. Pre-polymer was dissolved at a concentration of 25% (w/v) in dioxane. Once dissolved, it was mixed with 90–120 μm (at different ratios ranging from 40 to 90%) sieved NaCl salt until thoroughly combined. The resulting homogeneous slurry was set into molds and placed in a vacuum oven for 3 days at 120 °C for complete polymerization [40]. After the scaffold polymerized, no>6 mL volume of porous scaffolds were salt-leached in a 60 L DI water tub for 3 days with daily water exchanges. The scaffold was air dried and vacuum dried for 24 h each. Scaffolds were sterilized by autoclaving and stored in a desiccator until used.

3.2. Peptide synthesis and characterization

SLan and SLKr5 (Table 1) were synthesized with a CEM LibertyBlue solid phase peptide synthesizer with standard Fmoc chemistry (N-terminal acetylated and C-terminal amidated) [33,35]. The resulting crude peptide was subsequently cleaved with 0.25 mL each of H_2O, 3,6-dioxa-1,8-octanedithiol (DoDT), Triisopropylsilane (TIS) and 9.25 mL of Trifluoroacetic acid (TFA) for half an hour min at 37 °C in a water bath. Cold ether was used to crash out each peptide which was then vortexed with ether, centrifuged, and decanted. A peptide pellet was obtained drying overnight, which was resuspended in Milli-Q water at a concentration of 1 mg/mL. Once dissolved, the pH was adjusted to 7 and dialyzed with 2000 g/mol cutoff tubing (Spectra Por S/P 7 RC) against DI water for 3 days. Each of the purified peptides was frozen at −80℃ and lyophilized to yield a white cotton-like peptide product. The purity of the peptides was verified > 85% by an Agilent 1100 series High Performance Liquid Chromatography (HPLC) with an Agilent (Santa Clara, CA) C3 reverse phase column and the molecular weights of the peptides were verified with an Orbitrap Q Exactive LC/MS (Thermo Scientific, Waltham, MA).

3.3. Hydrogel preparation

The SLan and SLKr5 hydrogels were prepared by dissolving lyophilized peptide in 298 mM sucrose at a concentration of 20 mg/mL, mixed with equivalent volumes of HBSS buffer (containing the multivalent counterion phosphate).

3.4. SEM sample preparation and imaging

Sample preparation: 200 μL of SL-Kr5 or SLan hydrogels were fixed overnight with 2% glutaraldehyde (Sigma). The resulting crosslinked peptide hydrogels were washed with DI water thrice, and then ethanol dehydrated for 15 min each with increasing ethanol gradients (50%, 75%, 90%, 95%, 99%, and 100% twice). The ethanol dehydrated SLKr5 and SLan samples were critical point dried in a Tousimis AutoSamdri-795 (Rockville, Maryland) critical point dryer. Briefly, the chamber within the instrument was filled ¾ full with 100% ethanol, the samples were introduced with minimal/no exposure to air, and the chamber filled with ethanol. The chamber lid was closed, and cooled to 4 °C. The ethanol was continuously exchanged for liquid CO_2 for 20 min. The SLKr5 and SLan samples were maintained within liquid CO_2 for an hour followed by another 20 min liquid CO_2 purge. The samples were then brought to the CO_2 critical point (~1070 PSI) by raising the temperature to ~ 37–38 °C, followed by slow venting to atmospheric conditions. Samples were sputtered coated with a 8 nm of Au/Pd an EMS 150 TES sputter coater (Quorum, East Sussex, UK). Scanning electron microscopy performed using a JSM-7900 (Jeol, Peabody, MA) at 5.0 kV accelerating voltage and a working distance of 10 mm.

3.5. Incorporation of peptide hydrogels into porous scaffolds

The peptide hydrogels were incorporated into the POC scaffold by adjusting the centrifugation rate. At 1000 RCF, the scaffold collapsed at the bottom of the microcentrifuge tube. At lower speeds of 25–50 RCF, we observed the POC scaffold did not re-immerse with hydrogel. We optimized the incorporation of the hydrogel with the POC by centrifuging at 200 RCF for 5 min at 25 °C, and left the two-component scaffolds submerged in the microcentrifuge tube overnight before implantation.

3.6. Subcutaneous (Sub-Q) implantation

We followed NJIT-Rutgers Newark Institutional Animal Care and Use

Table 1
Sequences of relevant peptides used in this study.

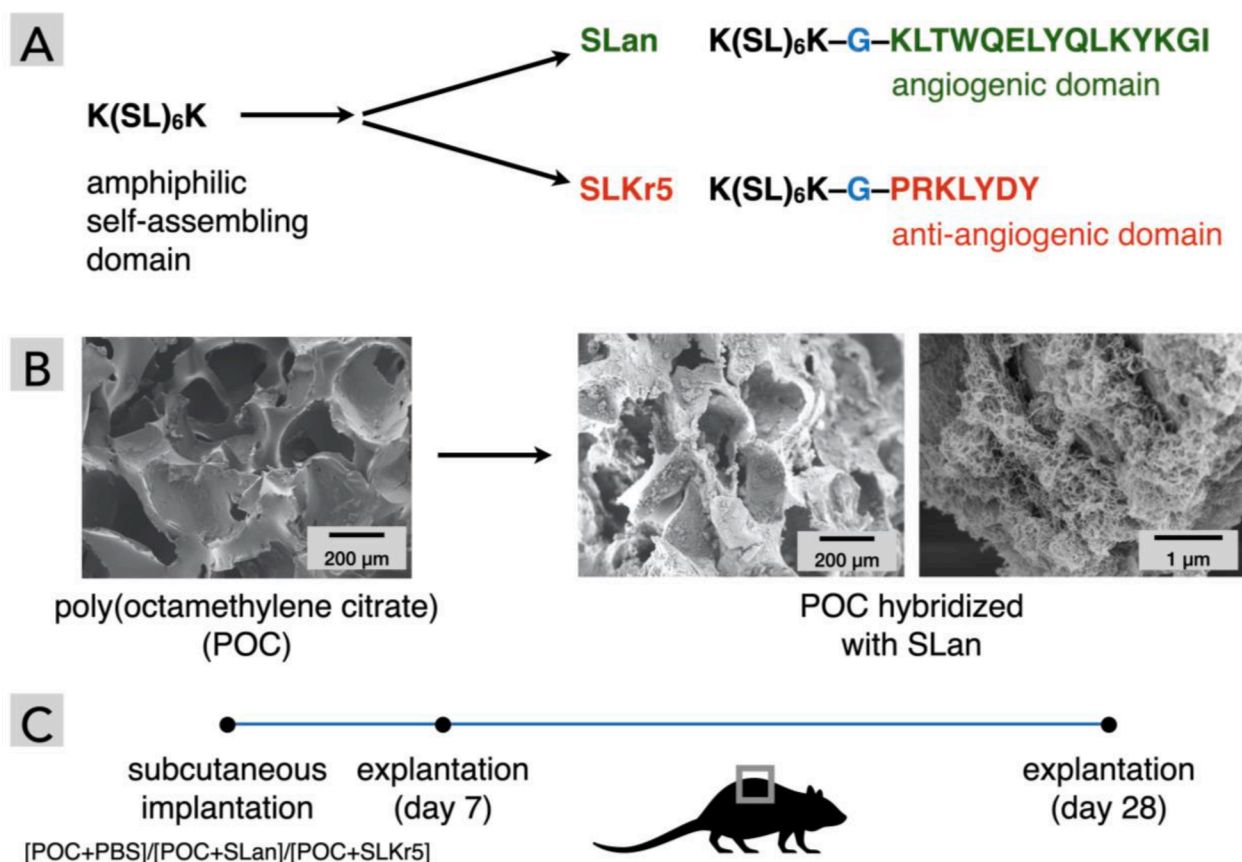| peptide	sequence	charge	format	conformation
SLan *angiogenic*	K(SL)$_6$K–G–KLTWQELYQLKYKGI	+4	hydrogel	β-sheet [35]
SLKr5 *anti-angiogenic*	K(SL)$_6$K–G–PRKLYDY	+3	hydrogel	β-sheet [33]

Fig. 1. Experimental design. (A) SLan and SLKr5 share sequence similarities, differing in their biofunctional moieties. (B) Microporous POC scaffolds before and after loading with the self-assembling peptide SLan, as observed in scanning electron microscopy (critical-point dried samples). The pores of the polymeric implant are ~ 100–250 μm. The hydrogels effectively fill these pores and form a nano-porous matrix inside these micro-pores (shown at two magnifications to highlight microscale and nanoscale features). (C) The scheme for testing biological response to POC scaffolds with and without self-assembling peptide hydrogels. Three types of scaffolds ([POC + PBS buffer], [POC + SLan], [POC + SLKr5]) were implanted in dorsal subcutaneous pockets of rats. A set of animals were sacrificed on day 7 to test short-term biological response. Rest of the implants were retrieved on day 28, to characterize long-term cellular infiltration and vascularization into the scaffolds by immunohistochemistry.

Committee (IACUC) and AALAC guidelines. Female Wistar rats (250–275 g) were used for dorsal subcutaneous implantation. POC samples were cut into 1 cm × 1 cm sponges that were embedded with phosphate buffered saline (PBS), SLKr5 [33], or SLan [35]. The rats were anesthetized using 2.5% isoflurane for induction and 1.5% isoflurane for maintenance, followed by shaving of dorsal regions and isopropanol and betadine sterile-prep of the surgical site. Small incisions were made 1 cm from each side of the thoracic or lumbar vertebrae (n = 4 sites per animal); the connective tissue (fascia) was cleared to create small 2 cm × 2 cm subcutaneous pockets. Composite scaffolds were placed under sterile conditions in subcutaneous pockets and the incisions were closed with Vetbond (3 M, Saint Paul, MN). At 7 and 28 days rats were sacrificed, and implant regions were excised. Harvested tissue sections were immediately fixed with 10% formalin. Samples were then processed by the histology core at the Rutgers Cancer Institute of New Jersey.

3.7. Immunohistochemical staining

The formalin fixed sections were ethanol series dehydrated, solvent exchanged for xylene, and then paraffin embedded using a tissue processor. Samples were blocked in paraffin, sectioned to 6–8 μm sections using a microtome, and stained using hematoxylin and eosin (H&E) or Masson's trichrome (MT) (SigmaAldrich, St. Louis, MO). For immunostaining staining, Rabbit anti-von Willebrand factor (vWF, Abcam, Cambridge, UK), Rabbit anti-rat α-smooth muscle actin (α-SMA, Gene-Tex, Irvine, CA) and 4′,6-diamidino-2-phenylindole (DAPI, Invitrogen,

Carlsbad, CA, USA) were used to stain endothelial cells, vascular smooth muscle cells, and nuclei, respectively. Donkey anti-rabbit was used as a secondary antibody for vWF staining and goat anti-rabbit as a secondary for α-SMA staining.

3.8. Characterization of histology/immunostaining

The cell density, infiltration, collagen deposition, blood vessel density and degree of regeneration for subcutaneous and pulp revascularization samples were calculated using QuPath. The polygon tool was used to draw along the border of the entire implant. The cell detection tool was selected to adjust threshold and minimum area parameters to get the most accurate count of cells (threshold usually set between 10 and 15 and area set between 5 and 10). Cell detection was executed with the region area and number of cells were recorded. The area was converted from pixels to mm based on image scale bar size conversion factors. The cell density was extrapolated by dividing the number of cells by outlined area in mm^2. The blood vessel density was calculated within each region and determined by dividing the number of blood vessels by outlined area in mm^2. Analyses were performed across all the regions within each slide (n = 4 regions per slide), and then all slides (n = 4 different implants per group) for 7 day and 28 day samples were averaged (Table 2, Table 3).

Table 2

Characterization of biological response after *in vivo* subcutaneous implantation.

formulation	time-points (days)	cellular infiltration	blood vessel formation
POC + PBS*neutral*	7 & 28	H&E	H&E, Masson, vWF, α-SMA
POC + SLan*angiogenic*	7 & 28	H&E	H&E, Masson, vWF, α-SMA
POC + SL-Kr5*anti-angiogenic*	7 & 28	H&E	H&E, Masson, vWF, α-SMA

4. Results:

SLan and SLKr5 have similar biophysical properties, as reported recently [33,35]. Both self-assemble into β-sheet nanofibers in aqueous solution at physiological conditions. The underlying nanofibrous architectures correspond to thixotropic hydrogels at the bulk scale [33,35]. Both hydrogels are reversibly shear-responsive, as demonstrated by oscillatory rheology (particularly with a shear recovery test) [33,35]. At high shear strain the viscoelastic hydrogels undergo liquefaction and promptly recover their elastic properties when the strain is lowered, resulting in reassembled hydrogels [33,35]. The thixotropic nature was observed with repeated strain cycles, demonstrating resilience of the self-assembled materials to retain this strain-dependent response. Thus, these biomaterials can be easily injected *in vivo*, where it can re-constitute into a stiff bolus. The rheological features of the hydrogels the consequences of the underlying non-covalent interactions (ionic bonds, hydrophobic interactions, etc.) that govern fibrillation and supramolecular cross-linking of the nanofibers into 3D meshes.

Integration of POC scaffolds with self-assembled peptide hydrogels (via simple centrifugation) yields hybrid micro-porous scaffolds suffused with nano-porous ECM-mimic peptide matrices (Fig. 1**B**). Our previous work has shown that nanofibrous architecture of SLan (**Fig. S1** in the Supporting Information) and SLKr5 hydrogels [33,35]. Hybridization of self-assembled hydrogels with POC scaffolds yields a two-component system with distinct material and chemical niches, which could be useful for segregation of infiltrating cells and may facilitate attachment and support of cells favoring different surface properties [41,42]. This system could act as a template for further application of such hydrogels for tuning the property of various porous implants.

To test the biological response to these two-component matrices, we selected an established subcutaneous implantation model in rats (Fig. 1**C**) [33,43]. We implanted three sets of scaffolds in rodent subcutaneous pockets: microporous POC filled with (a) PBS buffer ([POC + PBS]), (b) SLan hydrogel ([POC + SLan]), and (c) SLKr5 hydrogel ([POC + SLKr5]), to determine differing tissue infiltration into pores of the polymeric scaffolds. We explanted the implants at day 7 and day 28, and characterized cellular infiltration and blood vessel sprouting within the scaffolds by immunohistochemistry (Table 2, Table 3, Fig. 2, Fig. 3, **Fig. S2**,).

A typical feature of scaffold-induced foreign body response is the deposition of collagenous extracellular matrices around an implant

creating a thick vascularized coating, with minimal tissue ingrowth into a scaffold. While we observed some collagen deposition around all the implants at day 7 and day 28, there was enhanced tissue/collagen growth *within* hydrogel-filled scaffolds (both [POC + SLan] and [POC + SLKr5]) (Fig. 2, Fig. 3), pointing to increased bio-integration of the composite scaffolds. No foreign body giant cells, which are often indicative of adverse immune reaction to a scaffold, were observed in our samples — further demonstrating a lack of foreign body response at day 28 (see Fig. 3**E** for a magnified image of hydrogel filled pores).

[POC + PBS] scaffolds showed low cellular infiltration into ∼ 100–250 μm interconnected pores at both day 7 (Fig. 2**B**) and day 28 (Fig. 3**A**), with no tissue deposition within scaffolds over 28 days (Fig. 2, Fig. 3, Table 3). [POC + SLan] scaffolds showed rapid cellular infiltration (Fig. 2) with robust collagenous tissue deposition within scaffolds by 28 days (Fig. 2, Fig. 3). [POC + SLKr5] also showed significant cellular infiltration similar to [POC + SLan] (Fig. 2, Fig. 3), and similar ECM deposition within scaffolds (Fig. 3). There are clear differences in the tissue influx within specific pores between groups (Fig. 4, Table 3). By day 28, the full thickness of [POC + SLan] samples have tissue infiltrates (Fig. 3**E**, Fig. 4**C**, **Fig. S3–S6**). To further illustrate the degree of infiltration and comparative differences between scaffolds, we also conducted qualitative blinded analysis of histologic sections (Table 3).

We observed a striking difference in scaffold vascularization among the three implants, especially at the day 28 time-point (Fig. 3, **Fig. S4**, **Fig. S5**). The tissue infiltrates with [POC + SLan] scaffolds show numerous blood vessels (Fig. 3**E**) — the number of blood vessels was significantly higher than those in [POC + PBS] and [POC + SLKr5] implants (Fig. 4**C**). We decided to investigate whether the vessels formed were nascent leaky blood vessels without supporting mural cells, which are unstable and prone to resorption. We used a 3-panel imaging in immunohistochemistry that points out both endothelial cells (von Willebrand Factor vWF, red) and mural cells such as smooth muscle cells and pericytes (alpha-smooth muscle actin, α-SMA, green). Within scaffold pores, we observed large (15–50 μm) blood vessels lined by mural cells (as shown by colocalization of vWF and α-SMA (yellow) in Fig. 3**D**, **3F**, **Fig. S7**, **Fig. S8**). Lower vascularization in SLKr5-loaded scaffolds is congruent with our previous finding that the Kringle-5 like domain in SLKr5 imparts partial anti-angiogenic efficacy [33,34] but serves as a scaffold for tissue deposition (Fig. 4) [33].

5. Discussions:

5.1. Advantages of two-component scaffolds

Self-assembling peptide hydrogels formed via non-covalent interaction-driven liquid–liquid phase separation [44], can facilitate tissue regeneration [45–48]. Here we demonstrate that acellular nanofibrous peptide hydrogels can potentiate vascularization within microscopic polymeric pores *in vivo*.

Tissue-engineered scaffolds could be either solid scaffolds that need to be surgically implanted (e.g., covalently cross-linked polymeric materials) [30] or injectable scaffolds that can assemble *in vivo* (e.g.,
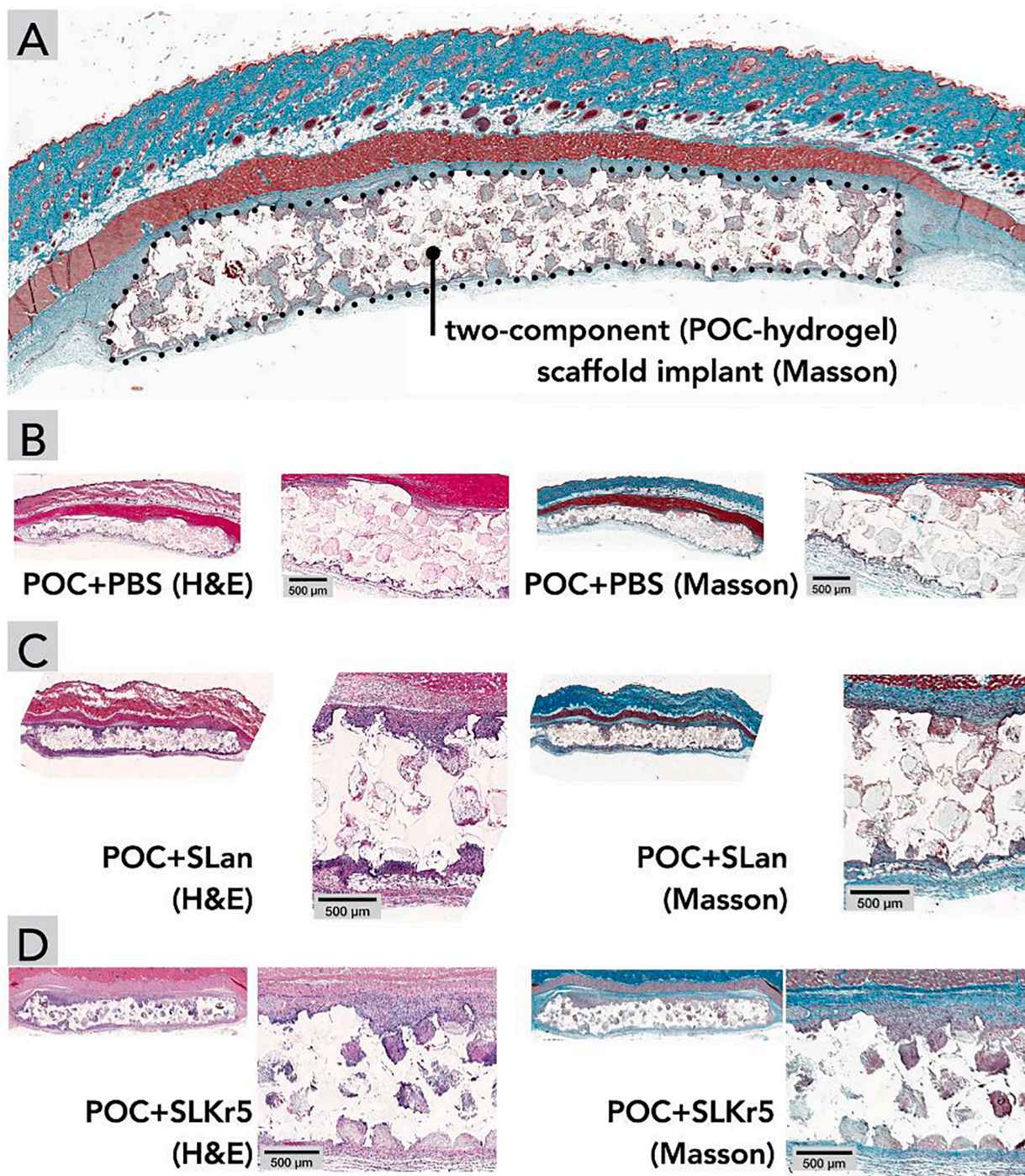
Table 3

Qualitative histomorphometric differences seen in POC scaffold implants.

	H&E Cellular infiltration	Central pores infiltrated	Trichrome Collagen deposition	Revascularization within pores	Fibrous encapsulation
7 Day					
POC + PBS	|	N/A	|	|	||
POC + SLKr5	|||	|||	|||	||	|
POC + SLan	||||	||||	||||	||||	|
28 Day					
POC + PBS	|	|	|	|	||
POC + SLKr5	||||	||||	||||	|||	|
POC + SLan	|||||	|||||	|||||	|||||	|

*qualitative measures graded on a scale of | - |||||.

Fig. 2. Subcutaneous implantations of scaffolds leading to cellular ingress at day 7. (A) Orientation of subcutaneous interconnected porous (100–250 μm) implants. Compared to (B) POC scaffolds with PBS, both (C) POC + SLan and (D) POC + SLKr5 scaffolds show higher cell infiltration, in H&E and Masson's Trichome staining.

noncovalently crosslinked supramolecular hydrogels) [19]. The former is more suitable for repairing hard tissues, whereas the latter can more easily integrate with soft tissues, as their material properties mimic corresponding tissue characteristics [2,33,35,43]. Tuning of material and biochemical properties of POC scaffolds [49,50] have yielded a class of citrate-based polymers with diverse applications in tissue engineering [30,49,51,52]. Our findings extend the use cases for such polymeric biomaterials and may lead to strategies for tunable promotion of peri-/intra-implant vascularization using such soft matrices within/on porous scaffold materials [53].

5.2. Controllable angiogenesis in vivo

Tissue engineering involves balancing trade-offs [12,54]. An inflammatory response is initiated by invasion of neutrophils and monocytes to an implant; a part of this ensuing cascade leads to the production of pro-angiogenic factors [15,47,55]. The resultant blood vessels then create channels for further infiltration of probing myeloid cells. This positive feedback loop, if not controlled, may lead to chronic inflammation. Thus, it may be desirable to develop tools to de-couple cellular infiltration from angiogenesis. The anti-angiogenic peptide hydrogel
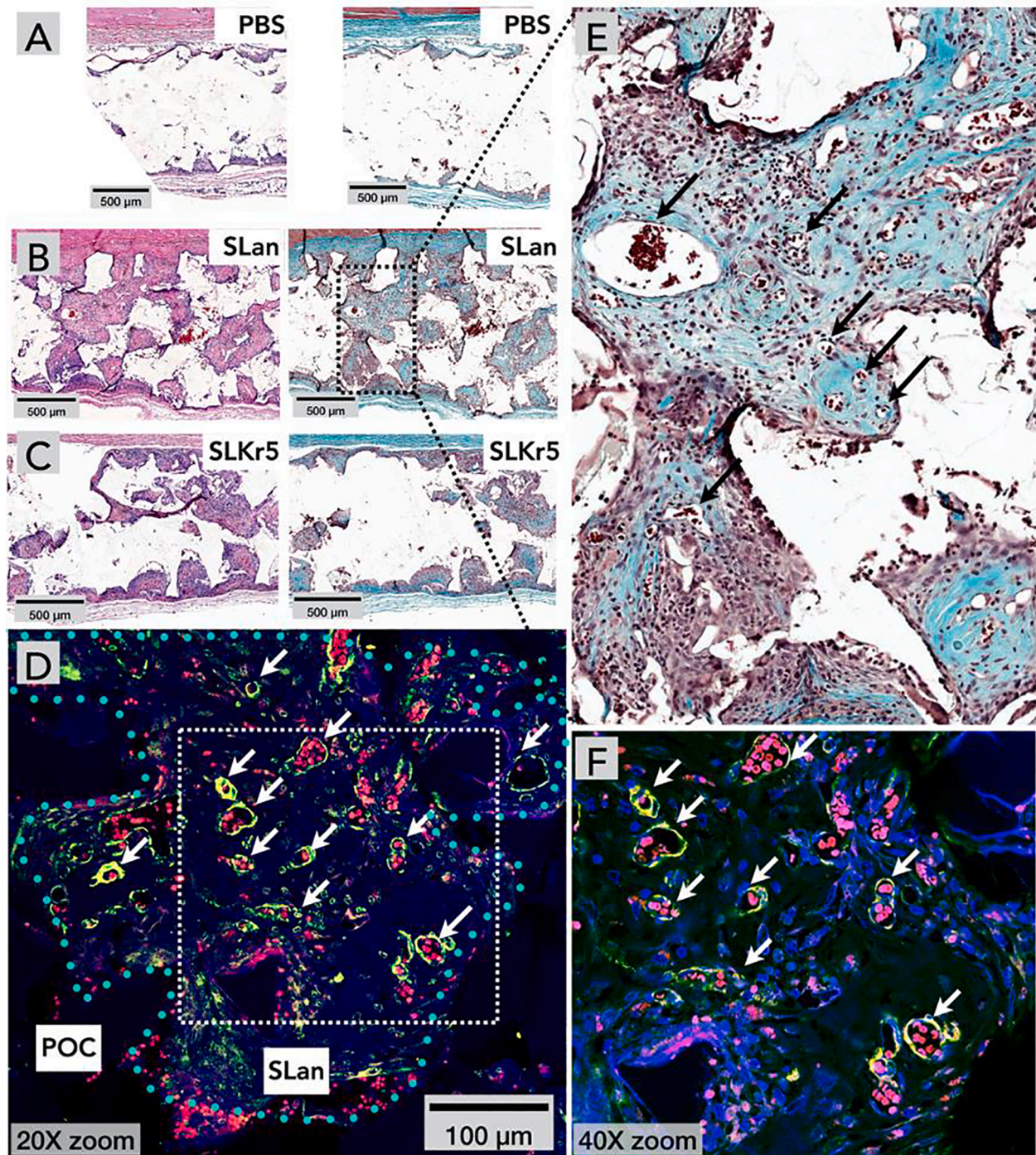
Fig. 3. Long-term (28 days) integration of two-component scaffolds with host tissue. H&E and Masson's Trichrome staining at 28 days for (A) [POC + PBS] show continued minimal infiltration compared to (B) [POC + SLan], which had significantly more vascularization than (C) [POC + SLKr5]. (D) SLan hydrogel incorporated into the POC scaffold pores mediated angiogenesis, as characterized by 3-panel immunostaining: vWF (endothelial cells, red), α-SMA (vascular smooth muscle cells, green), and DAPI (nuclei, blue) — the dotted line demarcates the soft hydrogel from the surrounding POC polymer matrix. Composites show ingress of cells and formation of new blood vessels inside the pores of the two-component [POC + SLan]. (E) A magnified section of panel B ([POC + SLan], Masson) shows large number of blood vessels in implant pores (pointed out by black arrows), (F) Confocal microscopy of the pores of panel D at higher zoom shows α-SMA + mature blood vessels (white arrows point to blood vessels).

SLKr5 is compatible with stromal cells, but prevents formation of blood vessels by endothelial cells [33]. Such anti-angiogenic hydrogels coupled with microporous scaffolds such as POC, may thus invite cell infiltration with minimal vascularization in the implant, adding an important regulatory tool in our design toolbox.

Two-component matrices such as the one developed here can bring together ECM-mimicking material/structural features of self-assembling peptide hydrogels and facile synthesis of polymeric scaffolds such as POC, providing a platform that retains synthetic simplicity and low batch-to-batch variability, while enabling *in vivo* implant integration [15–18].

Migration and formation of blood vessels into a two-component scaffold may depend on not only the chemical functionality embedded by design, but also on the material features, surface charge, and the
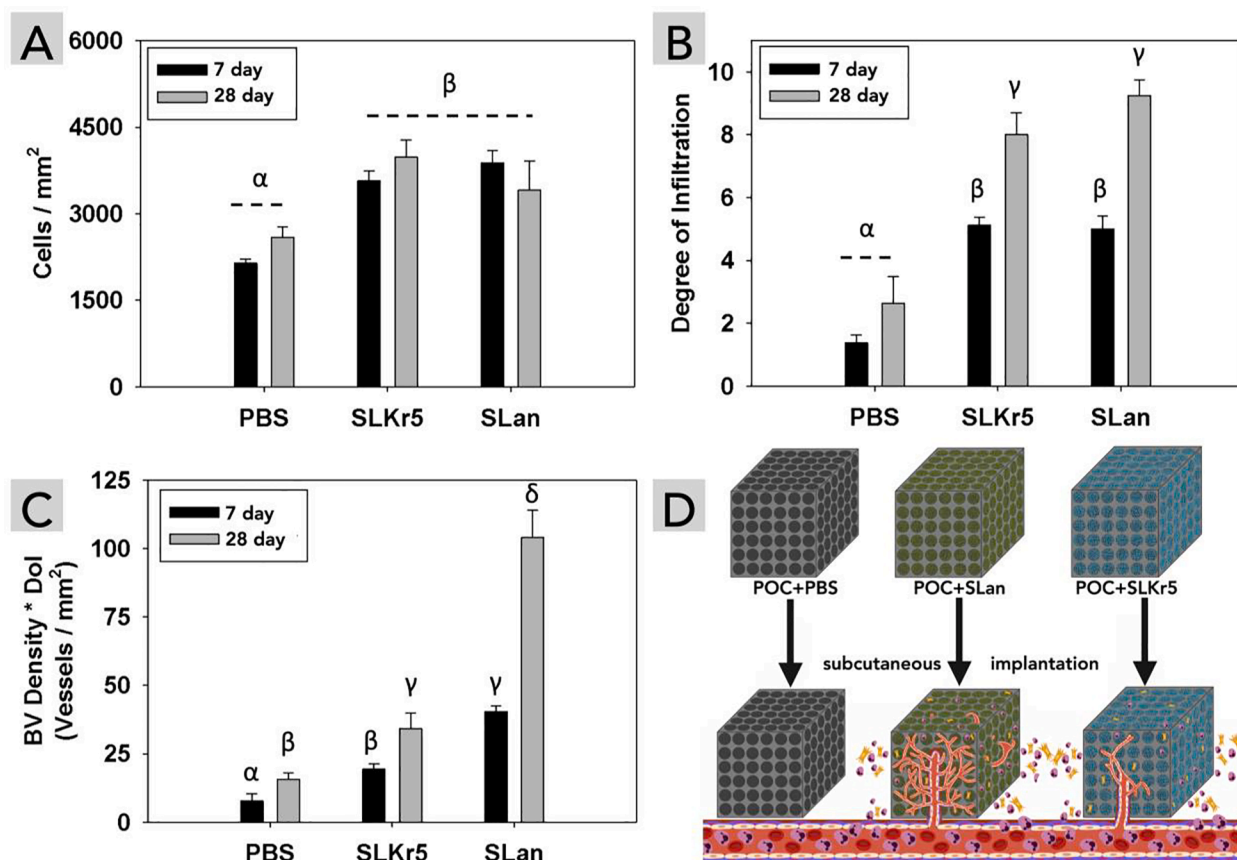
Fig. 4. Comparison of cellular infiltration and vascularization into scaffolds. (A–C) Self-assembling peptide hydrogels modulate cellular infiltration into two-component scaffolds and affect implant vascularization. Pristine POC scaffolds had low cellular infiltration and low density of blood vessels (degree of infiltration: scale of 0 refers to no cellular infiltration within the scaffold whereas a scale of 10 refers to complete cellular infiltration throughout the bulk of the scaffold). [POC + SLKr5] scaffolds had high levels of cell infiltration but low vascularization. [POC + SLan] scaffolds had similar cell infiltration as [POC + SLKr5], but had statistically higher vascular ingress, especially at day 28 timepoint (n = 4; different Greek letters indicate statistical significance between groups p < 0.05). (D) A scheme depicting cellular infiltration and vascularization into microporous scaffolds.

immune response triggered by the matrices [47]. Recruitment of myeloid cells to implanted peptide hydrogels may produce angiogenic cytokines, contributing to vascularization of the implant [47]. Similar mechanisms may be partly responsible for vascularizing the two-component scaffolds [POC + SLan] and [POC + SLKr5]. Despite similar formal charges on the building blocks (Table 1) and similar rheological properties [33,35], [POC + SLan] has dramatically higher extent of implant vascularization than [POC + SLKr5], by day 28 (Fig. 3, Fig. 4). We attribute the difference in the vascularization to the distinct bioactive moieties in the peptide sequences (Table 1, Fig. 1).

The anti-angiogenic peptide SLKr5 shares the central self-assembling domain with SLan and has the opposite biofunctional property (of blocking angiogenesis) — providing us an interesting pair of promoter/inhibitor dopants to influence biofunctional performance of POC scaffolds in opposing fashion (Fig. 3, Fig. 4). Such patterning of implanted scaffolds may offer an alternative way to provide pre-programmed signals to endogenous cells, in contrast to environmental stimuli [56]. A patterned acellular scaffold that is infiltrated by different populations of cells into segregated compartments or layers may be useful for functional tissue replacement.

The blood vessels formed inside [POC + SLan] scaffolds can be observed in both H&E and Masson's trichrome staining (Fig. 3). We confirmed that these blood vessels have a mature medial layer via staining for vascular smooth muscle cells (Fig. 3**D**), suggesting that they are mature non-transient structures. Such 25–50 μm blood vessels form within 28 days, preferentially within the angiogenic hydrogel-containing pockets of the POC implant (Fig. 3**E**). We demonstrate that

in vivo properties of hard polymeric scaffolds can be tuned by non-covalently doping with self-assembling peptide hydrogels.

5.3. Features of the acellular regenerative biomaterials

Polymeric implants can be ideal, from the standpoint of material properties, for repair and regeneration of tissues experiencing high shear rate — such as muscle, cartilage, and bone. Vascularizing these implants *in vivo* can improve their functional integration with the surrounding tissue. Such scaffolds can be great tools for tackling large volumetric tissue defects. In particular, the ability to rapidly generate robust vasculature in a wound bed would be advantageous for tissues with high metabolic rate, such as skeletal muscle [57,58]. Here we show that hybridization with an angiogenic peptide hydrogel can lead to rapid (in less than a month) formation of large, mature (25–50 μm, α-SMA+) blood vessels inside the central region of implants (over 2 mm in thickness), *without* exogenous cells or growth factors (Fig. 3**D–F**). Such scaffold-based signaling may lead to off-the-shelf acellular regenerative options [1,19,46,54], with low batch-to-batch variability and without pronounced foreign body response associated with synthetic scaffolds [15–18,47,59].

5.4. Limitations and future directions

We next aim to characterize the cellular infiltrates into these two-component scaffolds as a function of infiltrating vasculature and how they change temporally. We expect that the combination of cellular

infiltration and vascularization will enhance the efficacy of local/hematopoietic progenitor cells to stimulate tissue regeneration. Such studies would improve our understanding of the cell biology of vascularization in the implants and help us optimize the regenerative sequence post-injury.

The potential of our strategy can be extended even further by bioprinting scaffold/hydrogel pairs that allow a certain tissue formation (say, blood vessels), while blocking another (say, nerve fibers). In embryogenesis, such discrete structures form elegantly, but they are relatively difficult to recapitulate in laboratory conditions, especially as similar molecules guide both nerves and blood vessels (e.g., Netrins, VEGF-A, FGF-2, etc.) [60].

We have not yet studied the long-term (>6 months) biodegradability of these peptide hydrogels *in vivo*. It's possible that higher extents of vascularization may correlate with faster degradation rates. If such degradation coincides with concomitant deposition of extracellular matrix by the infiltrating cells, the integration of the hydrogel with the surrounding tissue may be favored, thus enhancing functional regeneration. Hydrogels that are degraded quickly can even be candidates as sacrificial components in multi-component regenerative scaffolds [19].

6. Conclusions

We have demonstrated a simple strategy of implanting two-component scaffolds *in vivo* for functional angiogenesis, where the components vary by chemical structure, material properties, porosity, and biological response. Self-assembling peptide nanofibers form ECM-mimetic matrices inside polymeric implants, instruct cellular infiltration, and guide angiogenic sprouting. Our study will be helpful for researchers interested in designing patterned biomimetic scaffolds that can engender component-specific biological response *in vivo*, resulting in segregated biomimetic tissue substitutes.

Declaration of Competing Interest

The authors declare that they have no known competing financial interests or personal relationships that could have appeared to influence the work reported in this paper.

Author Contributions

Z.S. and B.S. contributed equally. The manuscript was written through contributions of all authors. All authors have given approval to the final version of the manuscript.

Declaration of Competing Interest

J.Y. and V.A.K. have equity stakes in start-ups targeting commercializing similar technologies as described in this article.

Appendix A. Supplementary data

Supplementary data to this article can be found online at https://doi.org/10.1016/j.cej.2021.130145.

References:

[1] J.A. Burdick, R.L. Mauck, J.H. Gorman 3rd, R.C. Gorman, Acellular biomaterials: an evolving alternative to cell-based therapies, Sci Transl Med 5 (2013) 176ps174.

[2] B. Sarkar, X. Ma, A. Agas, Z. Siddiqui, P. Iglesias-Montoro, P.K. Nguyen, K.K. Kim, J. Haorah, V.A. Kumar, In vivo neuroprotective effect of a self-assembled peptide hydrogel, Chem. Eng. J. 408 (2021) 127295; doi: 127210.121016/j.cej.122020.127295.

[3] C.T. Johnson, M.C.P. Sok, K.E. Martin, P.P. Kalelkar, J.D. Caplin, E.A. Botchwey, A.J. Garcia, Lysostaphin and BMP-2 co-delivery reduces S. aureus infection and regenerates critical-sized segmental bone defects, Sci Adv 5 (2019) eaaw1228.

[4] V.A. Kumar, N.L. Taylor, S. Shi, B.K. Wang, A.A. Jalan, M.K. Kang, N. C. Wickremasinghe, J.D. Hartgerink, Highly Angiogenic Peptide Nanofibers, ACS Nano 9 (1) (2015) 860–868, https://doi.org/10.1021/nn506544b.

[5] V.A. Kumar, Q.i. Liu, N.C. Wickremasinghe, S. Shi, T.T. Cornwright, Y. Deng, A. Azares, A.N. Moore, A.M. Acevedo-Jake, N.R. Agudo, S.u. Pan, D.G. Woodside, P. Vanderslice, J.T. Willerson, R.A. Dixon, J.D. Hartgerink, Treatment of hind limb ischemia using angiogenic peptide nanofibers, Biomaterials 98 (2016) 113–119, https://doi.org/10.1016/j.biomaterials.2016.04.032.

[6] B.M. Sicari, J.P. Rubin, C.L. Dearth, M.T. Wolf, F. Ambrosio, M. Boninger, N. J. Turner, D.J. Weber, T.W. Simpson, A. Wyse, E.H. Brown, J.L. Dziki, L.E. Fisher, S. Brown, S.F. Badylak, An acellular biologic scaffold promotes skeletal muscle formation in mice and humans with volumetric muscle loss, Sci Transl Med 6 (2014) 234ra258.

[7] J.M. Grasman, D.M. Do, R.L. Page, G.D. Pins, Rapid release of growth factors regenerates force output in volumetric muscle loss injuries, Biomaterials 72 (2015) 49–60, https://doi.org/10.1016/j.biomaterials.2015.08.047.

[8] G.Y. Chen, G. Nuñez, Sterile inflammation: sensing and reacting to damage, Nat Rev Immunol 10 (12) (2010) 826–837, https://doi.org/10.1038/nri2873.

[9] M. Cicuéndez, J.C. Doadrio, A. Hernández, M.T. Portolés, I. Izquierdo-Barba, M. Vallet-Regí, Multifunctional pH sensitive 3D scaffolds for treatment and prevention of bone infection, Acta Biomaterialia 65 (2018) 450–461, https://doi.org/10.1016/j.actbio.2017.11.009.

[10] B. Sarkar, Z. Siddiqui, P.K. Nguyen, N. Dube, W. Fu, S. Park, S. Jaisinghani, R. Paul, S.D. Kozuch, D. Deng, P. Iglesias-Montoro, M. Li, D. Sabatino, D.S. Perlin, W. Zhang, J. Mondal, V.A. Kumar, Membrane-Disrupting Nanofibrous Peptide Hydrogels, ACS Biomater. Sci. Eng. 5 (9) (2019) 4657–4670, https://doi.org/10.1021/acsbiomaterials.9b00967.s001.

[11] R.K. Jain, P. Au, J. Tam, D.G. Duda, D. Fukumura, Engineering vascularized tissue, Nat Biotechnol 23 (7) (2005) 821–823, https://doi.org/10.1038/nbt0705-821.

[12] A. Atala, F.K. Kasper, A.G. Mikos, Engineering complex tissues, Sci Transl Med 4 (2012) 160rv112.

[13] H. Bae, A.S. Puranik, R. Gauvin, F. Edalat, B. Carrillo-Conde, N.A. Peppas, A. Khademhosseini, Building vascular networks, Sci Transl Med 4 (2012) 160ps123.

[14] F.A. Auger, L. Gibot, D. Lacroix, The Pivotal Role of Vascularization in Tissue Engineering, Annu. Rev. Biomed. Eng. 15 (1) (2013) 177–200, https://doi.org/10.1146/annurev-bioeng-071812-152428.

[15] K. Sadtler, M.T. Wolf, S. Ganguly, C.A. Moad, L. Chung, S. Majumdar, F. Housseau, D.M. Pardoll, J.H. Elisseeff, Divergent immune responses to synthetic and biological scaffolds, Biomaterials 192 (2019) 405–415, https://doi.org/10.1016/j.biomaterials.2018.11.002.

[16] S.D. Sommerfeld, C. Cherry, R.M. Schwab, L. Chung, D.R. Maestas Jr., P. Laffont, J. E. Stein, A. Tam, S. Ganguly, F. Housseau, J.M. Taube, D.M. Pardoll, P. Cahan, J. H. Elisseeff, Interleukin-36gamma-producing macrophages drive IL-17-mediated fibrosis, Sci Immunol 4 (2019).

[17] L. Chung, D.R. Maestas Jr., A. Lebid, A. Mageau, G.D. Rosson, X. Wu, M.T. Wolf, A. J. Tam, I. Vanderzee, X. Wang, J.I. Andorko, H. Zhang, R. Narain, K. Sadtler, H. Fan, D. Čiháková, C.J. Le Saux, F. Housseau, D.M. Pardoll, J.H. Elisseeff, Interleukin 17 and senescent cells regulate the foreign body response to synthetic material implants in mice and humans, Sci. Transl. Med. 12 (539) (2020) eaax3799, https://doi.org/10.1126/scitranslmed.aax3799.

[18] K. Sadtler, K. Estrellas, B.W. Allen, M.T. Wolf, H. Fan, A.J. Tam, C.H. Patel, B. S. Luber, H. Wang, K.R. Wagner, J.D. Powell, F. Housseau, D.M. Pardoll, J. H. Elisseeff, Developing a pro-regenerative biomaterial scaffold microenvironment requires T helper 2 cells, Science 352 (6283) (2016) 366–370, https://doi.org/10.1126/science:aad9272.

[19] B. Sarkar, P.K. Nguyen, W. Gao, A. Dondapati, Z. Siddiqui, V.A. Kumar, Angiogenic Self-Assembling Peptide Scaffolds for Functional Tissue Regeneration, Biomacromolecules 19 (9) (2018) 3597–3611, https://doi.org/10.1021/acs.biomac.8b01137.

[20] M.J. Webber, J. Tongers, C.J. Newcomb, K.-T. Marquardt, J. Bauersachs, D. W. Losordo, S.I. Stupp, Supramolecular nanostructures that mimic VEGF as a strategy for ischemic tissue repair, Proceedings of the National Academy of Sciences 108 (33) (2011) 13438–13443, https://doi.org/10.1073/pnas.1016546108.

[21] L. He, J. Zhou, M.o. Chen, C.-S. Lin, S.G. Kim, Y. Zhou, L. Xiang, M. Xie, H. Bai, H. Yao, C. Shi, P.G. Coelho, T.G. Bromage, B. Hu, N. Tovar, L. Witek, J. Wu, K. Chen, W. Gu, J. Zheng, T.-J. Sheu, J. Zhong, J. Wen, Y. Niu, B. Cheng, Q. Gong, D.M. Owens, M. Stanislauskas, J. Pei, G. Chotkowski, S. Wang, G. Yang, D. J. Zegarelli, X. Shi, D. Finkel, W. Zhang, J. Li, J. Cheng, D.P. Tarnow, X. Zhou, Z. Wang, X. Jiang, A. Romanov, D.W. Rowe, S. Wang, L. Ye, J. Ling, J. Mao, Parenchymal and stromal tissue regeneration of tooth organ by pivotal signals reinstated in decellularized matrix, Nat. Mater. 18 (6) (2019) 627–637, https://doi.org/10.1038/s41563-019-0368-6.

[22] Y.D. Lin, C.Y. Luo, Y.N. Hu, M.L. Yeh, Y.C. Hsueh, M.Y. Chang, D.C. Tsai, J. N. Wang, M.J. Tang, E.I. Wei, M.L. Springer, P.C. Hsieh, Instructive nanofiber scaffolds with VEGF create a microenvironment for arteriogenesis and cardiac repair, Sci Transl Med 4 (2012) 146ra109.

[23] J.D. Roh, R. Sawh-Martinez, M.P. Brennan, S.M. Jay, L. Devine, D.A. Rao, T. Yi, T. L. Mirensky, A. Nalbandian, B. Udelsman, N. Hibino, T. Shinoka, W.M. Saltzman, E. Snyder, T.R. Kyriakides, J.S. Pober, C.K. Breuer, Tissue-engineered vascular grafts transform into mature blood vessels via an inflammation-mediated process of vascular remodeling, Proceedings of the National Academy of Sciences 107 (10) (2010) 4669–4674, https://doi.org/10.1073/pnas.0911465107.

[24] A.O. Awojoodu, M.E. Ogle, L.S. Sefcik, D.T. Bowers, K. Martin, K.L. Brayman, K. R. Lynch, S.M. Peirce-Cottler, E. Botchwey, Sphingosine 1-phosphate receptor 3 regulates recruitment of anti-inflammatory monocytes to microvessels during implant arteriogenesis, Proc Natl Acad Sci USA 110 (34) (2013) 13785–13790, https://doi.org/10.1073/pnas.1221309110.

[25] B.J. Kwee, B.R. Seo, A.J. Najibi, A.W. Li, T.-Y. Shih, D. White, D.J. Mooney, Treating ischemia via recruitment of antigen-specific T cells, Sci. Adv. 5 (7) (2019) eaav6313, https://doi.org/10.1126/sciadv.aav6313.

[26] J. Yang, A.R. Webb, G.A. Ameer, Novel Citric Acid-Based Biodegradable Elastomers for Tissue Engineering, Adv. Mater. 16 (6) (2004) 511–516, https://doi.org/10.1002/adma.200306264.

[27] C.G. Jeong, S.J. Hollister, A comparison of the influence of material on in vitro cartilage tissue engineering with PCL, PGS, and POC 3D scaffold architecture seeded with chondrocytes, Biomaterials 31 (15) (2010) 4304–4312, https://doi.org/10.1016/j.biomaterials.2010.01.145.

[28] C.G. Jeong, H. Zhang, S.J. Hollister, Three-dimensional poly(1,8-octanediol-co-citrate) scaffold pore shape and permeability effects on sub-cutaneous in vivo chondrogenesis using primary chondrocytes, Acta Biomaterialia 7 (2) (2011) 505–514, https://doi.org/10.1016/j.actbio.2010.08.027.

[29] A.K. Sharma, P.V. Hota, D.J. Matoka, N.J. Fuller, D. Jandali, H. Thaker, G. A. Ameer, E.Y. Cheng, Urinary bladder smooth muscle regeneration utilizing bone marrow derived mesenchymal stem cell seeded elastomeric poly(1,8-octanediol-co-citrate) based thin films, Biomaterials 31 (24) (2010) 6207–6217, https://doi.org/10.1016/j.biomaterials.2010.04.054.

[30] C. Ma, X. Tian, J.P. Kim, D. Xie, X. Ao, D. Shan, Q. Lin, M.R. Hudock, X. Bai, J. Yang, Citrate-based materials fuel human stem cells by metabonegenic regulation, Proc Natl Acad Sci USA 115 (50) (2018) E11741–E11750, https://doi.org/10.1073/pnas.1813000115.

[31] V.A. Kumar, S. Shi, B.K. Wang, I.-C. Li, A.A. Jalan, B. Sarkar, N.C. Wickremasinghe, J.D. Hartgerink, Drug-Triggered and Cross-Linked Self-Assembling Nanofibrous Hydrogels, J. Am. Chem. Soc. 137 (14) (2015) 4823–4830, https://doi.org/10.1021/jacs.5b01549.

[32] V.A. Kumar, N.L. Taylor, S. Shi, N.C. Wickremasinghe, R.N. D'Souza, J. D. Hartgerink, Self-assembling multidomain peptides tailor biological responses through biphasic release, Biomaterials 52 (2015) 71–78, https://doi.org/10.1016/j.biomaterials.2015.01.079.

[33] P.K. Nguyen, B. Sarkar, Z. Siddiqui, M. McGowan, P. Iglesias-Montoro, S. Rachapudi, S. Kim, W. Gao, E.J. Lee, V.A. Kumar, Self-Assembly of an Antiangiogenic Nanofibrous Peptide Hydrogel, ACS Appl. Bio Mater. 1 (3) (2018) 865–870, https://doi.org/10.1021/acsabm.8b00283.s001.

[34] B. Sarkar, Z. Siddiqui, K.K. Kim, P.K. Nguyen, X. Reyes, T.J. McGill, V.A. Kumar, Implantable anti-angiogenic scaffolds for treatment of neovascular ocular pathologies, Drug Deliv. and Transl. Res. 10 (5) (2020) 1191–1202, https://doi.org/10.1007/s13346-020-00753-0.

[35] Z. Siddiqui, B. Sarkar, K.-K. Kim, N. Kadincesme, R. Paul, A. Kumar, A. Roy, M. Choudhury, J. Yang, E. Shimizu, Angiogenic Hydrogels for Dental Pulp Revascularization, Acta Biomater. (2021), https://doi.org/10.1016/j.actbio.2021.1003.1001.

[36] Y. Zheng, M.A. Roberts, Tissue engineering: Scalable vascularized implants, Nat Mater 15 (2016) 597–599.

[37] B. Zhang, M. Montgomery, M.D. Chamberlain, S. Ogawa, A. Korolj, A. Pahnke, L. Wells, S. Massé, J. Kim, L. Reis, A. Momen, S. Nunes, A.R. Wheeler, K. Nanthakumar, G. Keller, M. Sefton, M. Radisic, Biodegradable scaffold with built-in vasculature for organ-on-a-chip engineering and direct surgical anastomosis, Nature Mater 15 (6) (2016) 669–678, https://doi.org/10.1038/nmat4570.

[38] X. Li, B. Cho, R. Martin, M. Seu, C. Zhang, Z. Zhou, J.S. Choi, X. Jiang, L. Chen, G. Walia, J. Yan, M. Callanan, H. Liu, K. Colbert, J. Morrissette-McAlmon, W. Grayson, S. Reddy, J.M. Sacks, H.-Q. Mao, Nanofiber-hydrogel composite–mediated angiogenesis for soft tissue reconstruction, Sci. Transl. Med. 11 (490) (2019) eaau6210, https://doi.org/10.1126/scitranslmed.aau6210.

[39] H. Sekine, T. Shimizu, K. Sakaguchi, I. Dobashi, M. Wada, M. Yamato, E. Kobayashi, M. Umezu, T. Okano, In vitro fabrication of functional three-dimensional tissues with perfusable blood vessels, Nat Commun 4 (2013) 1399.

[40] H. Qiu, J. Yang, P. Kodali, J. Koh, G.A. Ameer, A citric acid-based hydroxyapatite composite for orthopedic implants, Biomaterials 27 (34) (2006) 5845–5854, https://doi.org/10.1016/j.biomaterials.2006.07.042.

[41] A.J. Engler, S. Sen, H.L. Sweeney, D.E. Discher, Matrix Elasticity Directs Stem Cell Lineage Specification, Cell 126 (4) (2006) 677–689, https://doi.org/10.1016/j.cell.2006.06.044.

[42] M.P. Lutolf, J.A. Hubbell, Synthetic biomaterials as instructive extracellular microenvironments for morphogenesis in tissue engineering, Nat Biotechnol 23 (1) (2005) 47–55, https://doi.org/10.1038/nbt1055.

[43] A.N. Moore, T.L. Lopez Silva, N.C. Carrejo, C.A. Origel Marmolejo, I.-C. Li, J. D. Hartgerink, Nanofibrous peptide hydrogel elicits angiogenesis and neurogenesis without drugs, proteins, or cells, Biomaterials 161 (2018) 154–163, https://doi.org/10.1016/j.biomaterials.2018.01.033.

[44] C. Yuan, A. Levin, W. Chen, R. Xing, Q. Zou, T.W. Herling, P.K. Challa, T.P. J. Knowles, X. Yan, Nucleation and Growth of Amino Acid and Peptide Supramolecular Polymers through Liquid–Liquid Phase Separation, Angew. Chem. Int. Ed. 58 (50) (2019) 18116–18123, https://doi.org/10.1002/anie.201911782.

[45] K.M. Galler, J.D. Hartgerink, A.C. Cavender, G. Schmalz, R.N. D'Souza, A Customized Self-Assembling Peptide Hydrogel for Dental Pulp Tissue Engineering, Tissue Engineering Part A 18 (1-2) (2012) 176–184, https://doi.org/10.1089/ten.tea.2011.0222.

[46] A.N. Moore, J.D. Hartgerink, Self-Assembling Multidomain Peptide Nanofibers for Delivery of Bioactive Molecules and Tissue Regeneration, Acc. Chem. Res. 50 (4) (2017) 714–722, https://doi.org/10.1021/acs.accounts.6b00553.s001.

[47] T.L. Lopez-Silva, D.G. Leach, A. Azares, I.C. Li, D.G. Woodside, J.D. Hartgerink, Chemical functionality of multidomain peptide hydrogels governs early host immune response, Biomaterials 231 (2020), 119667.

[48] J. Li, R. Xing, S. Bai, X. Yan, Recent advances of self-assembling peptide-based hydrogels for biomedical applications, Soft Matter 15 (8) (2019) 1704–1715, https://doi.org/10.1039/C8SM02573H.

[49] C. Ma, M.L. Kuzma, X. Bai, J. Yang, Biomaterial-Based Metabolic Regulation in Regenerative Engineering, Adv Sci (Weinh) 6 (2019) 1900819.

[50] J. Yang, D. Motlagh, A.R. Webb, G.A. Ameer, Novel Biphasic Elastomeric Scaffold for Small-Diameter Blood Vessel Tissue Engineering, Tissue Engineering 11 (11-12) (2005) 1876–1886, https://doi.org/10.1089/ten.2005.11.1876.

[51] C. Ma, E. Gerhard, Q. Lin, S. Xia, A.D. Armstrong, J. Yang, In vitro cytocompatibility evaluation of poly(octamethylene citrate) monomers toward their use in orthopedic regenerative engineering, Bioact Mater 3 (2018) 19–27.

[52] C. Ma, E. Gerhard, D.i. Lu, J. Yang, Citrate chemistry and biology for biomaterials design, Biomaterials 178 (2018) 383–400, https://doi.org/10.1016/j.biomaterials.2018.05.003.

[53] E.A. Phelps, N. Landázuri, P.M. Thulé, W.R. Taylor, A.J. García, Bioartificial matrices for therapeutic vascularization, Proc Natl Acad Sci USA 107 (8) (2010) 3323–3328, https://doi.org/10.1073/pnas.0905447107.

[54] M.J. Webber, E.A. Appel, E.W. Meijer, R. Langer, Supramolecular biomaterials, Nature Mater 15 (1) (2016) 13–26, https://doi.org/10.1038/nmat4474.

[55] A. Li, S. Dubey, M.L. Varney, B.J. Dave, R.K. Singh, IL-8 Directly Enhanced Endothelial Cell Survival, Proliferation, and Matrix Metalloproteinases Production and Regulated Angiogenesis, J Immunol 170 (6) (2003) 3369–3376, https://doi.org/10.4049/jimmunol.170.6.3369.

[56] B.A. Badeau, M.P. Comerford, C.K. Arakawa, J.A. Shadish, C.A. DeForest, Engineered modular biomaterial logic gates for environmentally triggered therapeutic delivery, Nature Chem 10 (3) (2018) 251–258, https://doi.org/10.1038/nchem.2917.

[57] K.H. Nakayama, C. Alcazar, G. Yang, M. Quarta, P. Paine, L. Doan, A. Davies, T. A. Rando, N.F. Huang, Rehabilitative exercise and spatially patterned nanofibrillar scaffolds enhance vascularization and innervation following volumetric muscle loss, NPJ Regen Med 3 (2018) 16.

[58] D. Gholobova, L. Terrie, M. Gerard, H. Declercq, L. Thorrez, Vascularization of tissue-engineered skeletal muscle constructs, Biomaterials 235 (2020), 119708.

[59] J.M. Anderson, A. Rodriguez, D.T. Chang, Foreign body reaction to biomaterials, Seminars in Immunology 20 (2) (2008) 86–100, https://doi.org/10.1016/j.smim.2007.11.004.

[60] T. Walchli, A. Wacker, K. Frei, L. Regli, M.E. Schwab, S.P. Hoerstrup, H. Gerhardt, B. Engelhardt, Wiring the Vascular Network with Neural Cues: A CNS Perspective, Neuron 87 (2015) 271–296.